JOURNAL OF GEOPHYSICAL RESEARCH, VOL. 106, NO. B11, PAGES 26,467–26,482, NOVEMBER 10, 2001

Dynamic modeling of the 1992 Landers earthquake

Sophie Peyrat

Laboratoire de Géologie, École Normale Supérieure, Paris, France

Kim Olsen

Institute for Crustal Studies, University of California, Santa Barbara, California, USA

Raúl Madariaga

Laboratoire de Géologie, École Normale Supérieure, Paris, France

Abstract. We have used observed band-pass filtered accelerograms and a previously determined slip distribution to invert for the dynamic rupture propagation of the 1992 Landers earthquake. In our simulations, dynamic rupture grows under the simultaneous control of initial stress and rupture resistance by friction, which we modeled using a simple slip-weakening law. We used a simplified Landers fault model where the fault segments were combined into a single vertical, planar fault. By trial and error we modified an initial stress field, inferred from the kinematic slip distribution proposed by *Wald and Heaton* [1994], until dynamic rupture generated a rupture history and final slip distribution that approximately matched those determined by the kinematic inversion. We found that rupture propagation was extremely sensitive to small changes in the distribution of prestress and that a delicate balance with energy release rate controls the average rupture speed. For the inversion we generated synthetic 0.5 Hz ground displacements using an efficient Green's function propagator method (AXITRA). This method enables us to propagate the radiation generated by the dynamic rupture to distances greater than those feasible using the finite difference method. The dynamic model built by trial-and-error inversion provides a very satisfactory fit between synthetics and strong motion data. We validated this model using records from stations used in the slip inversion as well as some which were not included. We also inverted for a complementary model that fits the data just as well but in which the initial stress was perfectly uniform while rupture resistance was heterogeneous. This demonstrates that inversion of ground motion is nonunique.

1. Introduction

The June 28 1992, Landers earthquake is one of the largest, well-recorded earthquakes in California. This earthquake occurred in the Mojave Desert in southern California on a series of right-lateral strike-slip faults within the Eastern California Shear Zone. Its focal mechanism, right-lateral strike slip, was consistent with the regional deformation of the Mojave block [*Unruh et al.*, 1994].

The high quality and variety of data available for this event provided an unprecedented opportunity to study its rupture process in detail. For example, *Wald and Heaton* [1994] combined geodetic data with seismic data to infer a distributed fault model and to retrieve the kinematic rupture history. *Cohee and Beroza* [1994] modeled the rupture process using an empirical Green's function approach to obtain similar results. *Cotton and Campillo* [1995] used frequency domain inversion of strong motion data in order to constrain the space-time dependence of slip on the fault. *Hernandez et al.* [1999] studied the rupture process of the Landers earthquake through simultaneous inversion of interferometric synthetic aperture radar (InSAR) data, Global Positioning System measurements, and strong motion data. Finally, *Day et al.* [1998] and *Bouchon et al.* [1998] determined the space time variation of shear stress on the fault from slip models obtained by kinematic inversion.

Generally, previous attempts at modeling the Landers earthquake were kinematic, except for *Olsen et al.* [1997]. Such models contain some mechanical inconsistencies, the most important one being that in kinematic models, rupture is forced to propagate at more or less predetermined speeds or within a certain range of speeds. Dynamic models, on the other hand, should satisfy more realistic and well-posed frictional conditions on the fault surface, and in particular, the motion of the rupture front should be determined from the simultaneous control of the initial load and rupture resistance by friction. Several attempts have been made to reconstruct the stress field acting on earthquake faults directly from

Paper number 2001JB000205.
0148-0227/01/2001JB000205$09.00

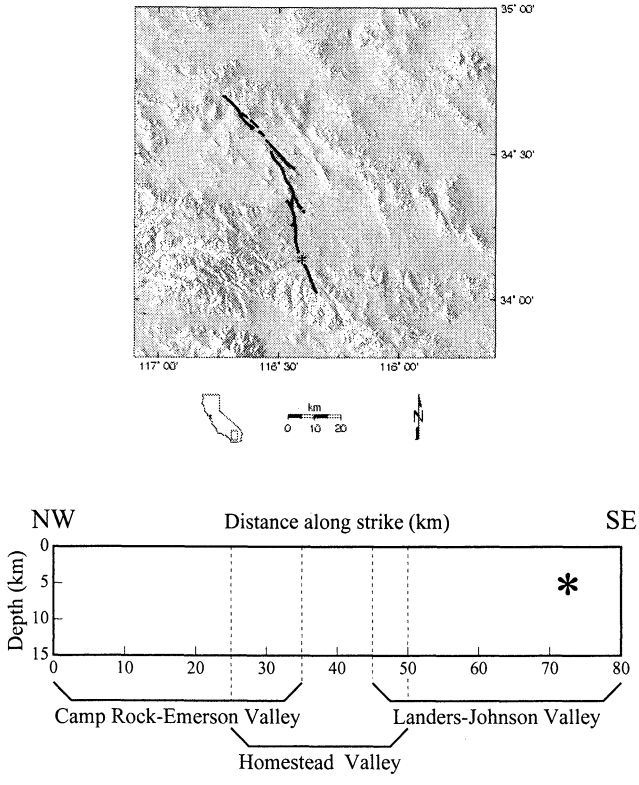

Figure 1. The Landers earthquake fault (80 km long, and extending from the surface to a depth of 16 km) was divided by *Wald and Heaton* [1994] into three segments: the Landers Johnson Valley segment to the south where the hypocenter (star) is located, the Homestead Valley segment in the central part of the fault, and the Camp Rock Emerson Valley segment to the north.

kinematic rupture inversions [*Fukuyama and Mikumo*, 1993; *Quin*, 1990; *Miyatake*, 1992; *Beroza and Mikumo*, 1996; *Bouchon*, 1997; *Ide and Takeo*, 1997]. These authors computed the distribution of shear stress change over the fault from the slip distribution determined by waveform inversions and constructed a quasi-dynamical model of the rupture process.

The faults that ruptured during the Landers earthquake were very complex: they contained several nonplanar segments described in detail by *Sieh et al.* [1993]. Inverting a dynamic rupture model with detailed fault geometry is not possible with our current computer capabilities. Most seismologists, following *Wald and Heaton* [1994] have used a three-segment geometry, the Landers Johnson Valley segment to the south where the hypocenter is located, the Homestead Valley segment in the central part of the fault, and the Camp Rock Emerson Valley segment to the north (see Figure 1). Because of current computational limitations of our finite difference method we simplified the *Wald and Heaton* [1994] model even further, assuming that the fault that ruptured during the Landers earthquake was a single vertical segment, 80 km long, and extending from the surface to a depth of 15 km (see Figure 1).

The kinematic rupture history of the Landers earthquake is now well constrained, and it occurred within a network of accelerometers that enabled detailed modeling of its rupture characteristics. Therefore this earthquake is an appropriate test for dynamic inversion. In a first attempt at constructing a dynamic model of the Landers earthquake, *Olsen et al.* [1997] studied the frictional conditions under which rupture could propagate or not and then modeled the dynamic rupture process for the initial stress field obtained from the slip distribution determined by *Wald and Heaton* [1994]. *Olsen et al.* [1997] also modeled the radiation from their dynamic rupture and validated the simulation against four strong motion records but did not attempt to fit the observed ground displacements. Recently, *Aochi* [1999] simulated the rupture process of the Landers earthquake on a nonplanar fault model using a three-dimensional (3-D) boundary integral equation method but under the restricted assumption of uniform initial stress and friction.

The aim in the present paper is more ambitious: we will invert for the initial shear stress field on the fault from the observed ground motion and the seismic moment determined by *Wald and Heaton* [1994]. Because seismic waves are only sensitive to stress change, the inverse problem of earthquake dynamics is ill posed. In a first inversion we assumed that rupture was entirely controlled by the initial stress field and that friction on the fault was uniformly distributed. This inversion produced what we call an asperity model which is clearly an extreme assumption, so that our result may be considered an end model among the family of properly posed mechanical models that simulate the ground motion generated by the Landers earthquake. Our goal is to find what we consider the simplest dynamic models that satisfy all the seismological observations. Many other models can be inverted from these ground motion and slip distribution. For example, we will invert for another end model in which the initial stress is uniform but friction is heterogeneous [*Peyrat et al.*, 2000]. Other possible models include segmented faults of the type considered by *Harris and Day.* [1999], *Aochi and Fukuyama* [2000], or *Aochi et al.* [2000].

2. Numerical Modeling Method and Friction Law

We model the Landers earthquake as the propagation of a spontaneous rupture along a simple planar fault. The velocity-stress formulation of linear elastodynamics can be written as

$$\begin{aligned} \rho\frac{\partial \mathbf{v}}{\partial t} &= \nabla\cdot\boldsymbol{\sigma}+\mathbf{f} \\ \frac{\partial \boldsymbol{\sigma}}{\partial t} &= \lambda\nabla\cdot\mathbf{v}\mathbf{I}+\mu[(\nabla\mathbf{v})+(\nabla\mathbf{v})^T]+\dot{\mathbf{m}}, \end{aligned} \quad (1)$$

where $\mathbf{v}$ is the velocity vector, $\boldsymbol{\sigma}$ is the stress tensor, ρ is the density of the medium, λ and μ are the elastic moduli, $\boldsymbol{I}$ is the identity matrix of rank 3, and $\mathbf{f}$ and $\dot{\mathbf{m}}$ are the force and moment rate distributions, respectively. We solve (1) using a fourth-order staggered-grid finite difference (FD) method in a three-dimensional medium.

In this method, introduced by *Madariaga* [1976] and *Virieux and Madariaga* [1982] and later improved by *Olsen*

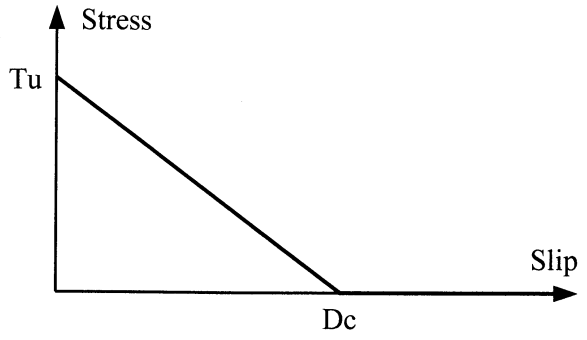

Figure 2. Slip-weakening friction law. Slip is zero until the stress reaches a peak value (the yield stress T_u), at which slip starts to increase from zero and stress decreases linearly to zero. Slip weakening is measured by D_c, the slip-weakening distance.

[1994] and *Madariaga et al.* [1998], stresses and particle velocities are computed on a staggered grid, using a thick fault zone that preserves the symmetries of stresses and velocities across the fault. This method, using a fourth-order approximation to spatial derivatives, successfully eliminates numerical instabilities in second-order methods reported by *Virieux and Madariaga* [1982]. Equation (1) is combined with the following boundary conditions: a free surface boundary condition at the top of the fault, with absorbing boundary conditions introduced at the grid edges to eliminate numerical artifacts. Finally, the fault is modeled as an internal boundary on which stress is related to slip by a friction law:

$$\sigma_{xy} = T(D, \theta), \tag{2}$$

where σ_{xy} is the shear stress on the fault located on a plane of normal y. The axis x is taken along the fault trace. T is the traction between the fault walls, D is the slip across the fault, and θ represents any number of internal variables.

The friction law must contain a finite length scale that controls the behavior of the rupture front, avoid stress singularities at the tip of the crack, and account for finite rupture energy flow [*Ida*, 1972]. Thus rupture propagation is controlled by the properties of this friction law: friction controls the initiation, the development of rupture, and the healing of the fault. The friction law used in this study (Figure 2) is the simple slip-weakening law

$$T(D) = \begin{cases} T_u\left(1 - \frac{D}{D_c}\right) + T_f & D < D_c \\ T_f & D > D_c \end{cases}, \tag{3}$$

where T_f is the kinematic friction at high slip and D_c is the slip-weakening displacement. In the slip-weakening model (3), T is assumed to be a function only of slip D; no internal variables are used. This friction law was introduced by *Ida* [1972] and later numerically applied to dynamic rupture propagation by *Andrews* [1976] for a two-dimensional shear crack and by *Day* [1982] for a three-dimensional crack. Slip is zero until the stress reaches a peak value (T_u); then it starts to increase while, simultaneously, stress decreases linearly to T_f over the slip weakening distance D_c. Energy release rate at the rupture front G for such a model is defined by

$$G = \int_0^{D_c} [T(D) - T_f] dD = \frac{1}{2}(T_u - T_f) D_c \tag{4}$$

[see, e.g., *Freund*, 1989]. For additional details of the numerical method we refer to *Madariaga et al.* [1998].

The first set of simulations presented in this study are conducted under the assumption that both friction parameters D_c and T_u are constant and independent of position on the fault. We are, of course, aware that this is an approximation, but we want to find the simplest model that is dynamically correct and satisfies observations. In this case we can also assume without loss of generality that $T_f = 0$ since earthquake slip is insensitive to the absolute stress level.

Since we assume uniform frictional properties along the fault, dynamic rupture is completely controlled by the initial stress on the fault before rupture starts. *Olsen et al.* [1997] generated an initial stress model from some simple considerations about initial and final stress on the fault, based on the combined kinematic model of *Wald and Heaton* [1994]. Figure 3 shows the initial stress distribution calculated by *Olsen et al.* [1997], and it shows large areas of almost homogeneous high stress surrounded by narrow regions of low stress. In our iterative inversion method we used the initial stress field determined by *Olsen et al.* [1997] as the initial model. Our aim was to modify the initial stress field by iterative inversion of the observed ground motion. In our search for the initial stress field we constrained the prestress on the fault to values just below the yield stress T_u (95% of T_u) to prevent rupture from starting at several locations simultane-

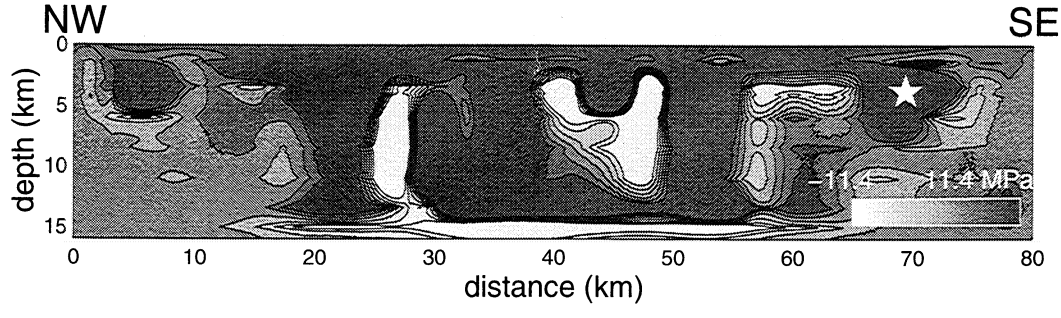

Figure 3. Initial stress field on the Landers fault constructed by *Olsen et al.* [1997] from the static field obtained from kinematic slip inversion [*Wald and Heaton*, 1994]. Contour interval is 3.8 MPa.

Table 1. One-Dimensional Model Used in Numerical Modeling

Depth, km	V_p, km/s	V_s, km/s	ρ, g/cm^3	Q_p	Q_s
0.0	3.8	1.98	2.30	100	30
1.5	5.5	3.15	2.60	600	300
4.0	6.2	3.52	2.70	600	300
26.0	6.8	3.83	2.87	600	300
32.0	8.0	4.64	3.50	600	300

V_p and Q_p are the P wave velocity and quality factor, respectively, V_s and Q_s are the S wave velocity and quality factor, respectively, and ρ is the density of the medium.

ously. The initiation of the rupture was forced by lowering the yield stress in a small patch in the region surrounding the hypocenter.

Because of numerical limitations of our finite difference method we assumed that the fault was planar and slip occurred only in the direction parallel to the applied shear stress, i.e., in the long direction of the strike-slip fault, so that slip becomes a scalar in the simulation to reduce the number of rupture parameters. This assumption is consistent with kinematic source inversion results for this event. The temporal discretization was taken as 0.0125 s, the grid spacing was taken as 200 m, and the fault was 80 km long by 16 km wide. We used the same regional one-dimensional model of velocities and densities (see Table 1) as the one used in the kinematic inversion by *Wald and Heaton* [1994].

3. Influence of Prestress

Olsen et al. [1997] found that the rupture speed and healing on the modeled Landers fault were critically determined by the level of the yield stress and the slip-weakening distance in the friction law. In particular, their study suggested that earthquakes are critical phenomena, occurring only for a limited range of rupture resistance. Recently, *Madariaga and Olsen* [2000] identified a nondimensional parameter

$$\kappa = T_e^2 W/\mu(T_u - T_f)D_c \tag{5}$$

that controls rupture, where W is the width of the fault, T_e is the effective shear stress (an average stress drop), T_u is the yield stress, and D_c is the slip-weakening distance. This parameter roughly represents the ratio of the available strain energy ($U \simeq T_e^2 W/\mu$) to the energy release rate G (4). Rupture only grows beyond the initial asperity when $\kappa > \kappa_c$, where κ_c is the critical value that can be found from the previous studies by *Andrews* [1976] and *Day* [1982]. Let us remark that κ is completely independent of the residual stress T_f, as it should be. Depending of the geometry, *Madariaga and Olsen* [2000] found that κ_c is of the order of 0.5-1.

We can now estimate the value of κ for the Landers models. We selected the appropriate friction parameters that allow rupture propagation ($D_c = 0.8$ m, $T_u - T_f = 12.5$ MPa, so that $G = 5$ MJ/m^2), which are very similar to the values used by *Olsen et al.* [1997]. While D_c and T_u cannot be determined independently, G is very well determined. As discussed by *Olsen et al.* [1997], for $G < 5$ MJ/m^2, rupture does not propagate beyond the hypocenter, while for values significantly larger than 5 MJ/m^2, rupture propagates at supershear speeds so that it is impossible to fit the observed duration of ground displacement. We adopt a value of $T_u - T_f = 12.5$ MPa because this is an upper bound for the stress drops we computed from the slip model proposed by *Wald and Heaton* [1994]. These values are of the same order of magnitude as those computed by *Bouchon et al.* [1998] and *Guatteri and Spudich* [2000] from other models of slip for the Landers earthquake. The latter authors discuss the resolution of kinematic inversions in which rise time is considered as an independent parameter. Rise time is not independent in our work; it is a result of the slip-weakening law.

From the slip distribution determined by *Wald and Heaton* [1994], *Olsen et al.* [1997] determined the distribution of stress drop $\Delta\sigma_{xy}(x, y)$, from which the average stress drop $T_e = 1/S \int_S \sigma_{xy}(x, y)dxdy$ can be computed. Here S is the area of the fault plane that slipped during the Landers earthquake. We found an average stress drop $T_e = 4$ MPa, using an average value of the elastic rigidity of $\mu = 3.37 \times 10^{10}$ Nm. For the fault width $W = 16$ km, $\kappa \simeq 0.72$, which is very close to the critical value for a rectangular fault $\kappa_c \simeq 0.76$ obtained by *Madariaga and Olsen* [2000].

Let us first demonstrate that rupture propagation is extremely sensitive to the initial stress (a typical effect of criticality). Plate 1 shows the time evolution of the rupture for three different initial stress fields. The main differences are in the value of the initial shear stress in the region near the hypocenter. The snapshots represent the state of stress and slip rate on the fault at five intervals equally spaced in time. Rupture propagation is associated with a stress decrease (green in Plate 1). Plate 1b corresponds to the initial condition shown in Figure 3, which is the stress field originally used by *Olsen et al.* [1997]. In this case the rupture starts to propagate very slowly following a narrow path near the free surface. We modified the initial stress of Plate 1a in the region near the surface, in the area just above the hypocenter. We lowered the stress (near 0 MPa) in order to avoid propagation along this path, so that rupture starts to propagate but stops after ~6 s because stress is too low in the surrounding regions. Next, the initial stress in the region below the hypocenter (Plate 1c) was increased from 7 to 11.4 MPa in order to allow the rupture to propagate. We observe essentially three categories of rupture propagation. Rupture in the first category does not propagate much beyond the area immediately around the nucleation (this case is not shown in Plate 1). In the second category, rupture starts to propagate but stops rapidly (Plate 1a). Thus critical conditions are required to promote rupture propagation from the initial nucleation patch to the remaining part of the fault and to avoid premature rupture arrest. In the third category (Plate 1b and 1c), soon after the initiation, rupture propagates along a complex path with variable speed. These models produce

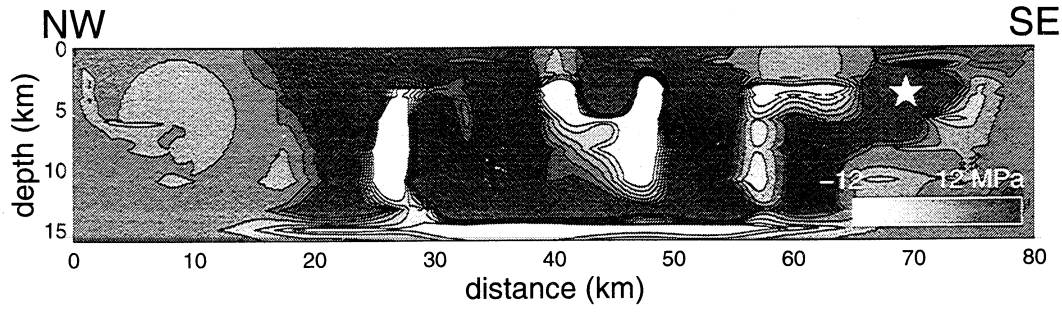

Figure 4. Initial stress distribution of the 1992 Landers earthquake determined by our trial-and-error inversion method. Contour interval is 4 MPa.

both a propagating rupture and preserve some level of inhomogeneity in the final slip distribution, in agreement with kinematic results.

In summary, rupture propagation is extremely sensitive to small changes in the distribution of prestress. Since we assumed constant friction properties on the fault, the rupture history in our model is entirely controlled by changing the prestress distribution.

4. Results

4.1. Final Model

We have seen that under our assumptions, rupture propagation is critically controlled by the initial stress distribution. Thus the observed ground motion is determined by a very nonlinear relation with the initial stress field. It is very unlikely that linearized inversion will work for this problem; only fully nonlinear inversion methods like Monte Carlo or genetic algorithms have any chance to find a reasonable model. However, since rupture is almost critical, the initial stress distribution can be modified to produce a rupture process that is as close as possible to that of the kinematic model of *Wald and Heaton* [1994]. This is a tedious process, but very quickly, we learned to steer rupture along the fault by modifying the stress field. Therefore we modified the prestress determined by *Olsen et al.* [1997] by trial and error in order to generate a rupture history similar to the kinematic results by *Wald and Heaton* [1994]. After several hundreds of dynamic models, we found the initial stress distribution shown in Figure 4. The main differences with the initial stress model of *Olsen et al.* [1997] is that the values are lower in the region above the hypocenter, while they had to be increased below the hypocenter. Moreover, the initial stress had to be decreased in the final region of the fault (to the northwest) in order to avoid a run-away supershear rupture that would be incompatible with observed ground motion.

Plates 2a and 2b show a comparison between the results of the kinematic and the dynamic rupture simulation on the fault. Each snapshot depicts the preferred horizontal slip rate during 1 s time slices. In Plate 2a the kinematic model was recomputed from *Wald and Heaton*'s [1994] tables. In the case of the dynamic model (Plate 2b), soon after initiation, rupture propagates slowly downward. After 7 s, it appears that the rupture almost dies out, but soon after, it suddenly accelerates upward. It again slows down at 11 s before jumping to the northern part of the fault and continues onward. Finally, the rupture terminates on the shallow northwestern part of the fault after ~21 s in agreement with the kinematic inversion. The rupture shows a confined band of slip propagating unilaterally toward the northeast along the fault, as pointed out by *Wald and Heaton* [1994]. The finite width of the fault promotes the formation of a pulse by confining the rupture laterally, preventing the development of a crack-like rupture. The main differences between the kinematic and dynamic models occur within the first 10 s of propagation. The slip rate peak at 5-6 s for the kinematic model appears later (at 9 s) for the dynamic model. Nevertheless, the main part of the rupture history (13-17 s) is very similar for the two models.

The propagation of the rupture front can also be observed in Plate 2c, which shows the temporal variation of shear stress on the fault. The propagation is associated with a stress decrease (green), and the rupture only propagates in regions of high stress (red). The stress relaxation on the fault automatically creates a stress increase concentrated near the rupture front, which tends to facilitate the growth of rupture. The propagation of the rupture front, in the case of a heterogeneous distribution of stress, is then determined by the immediate history of rupture and by the state of stress over all nearby points. The rupture front is slowed down and delayed along the Landers fault. A strong connectivity of high stress patches is required in order to promote rupture propagation from the initial nucleation point to the remaining part of the fault as shown by *Nielsen and Olsen* [2000] for the Northridge earthquake, so that the rupture is able to progress through an almost uninterrupted high-stress path. When rupture encounters a localized low-stress patch with surrounding regions of high stress sufficiently narrow, rupture is slowed down and jumps to a nearby larger area of high stress (at 9 s). We can also see a time delay of a few seconds from the time of the arrival of the rupture front and the time that rupture continues onward (after 6-8 s). A decrease of the rupture velocity followed by an acceleration corresponds to a large stress buildup (e.g., after 13 s). Thus, in our model the complex rupture path and the healing are consequences

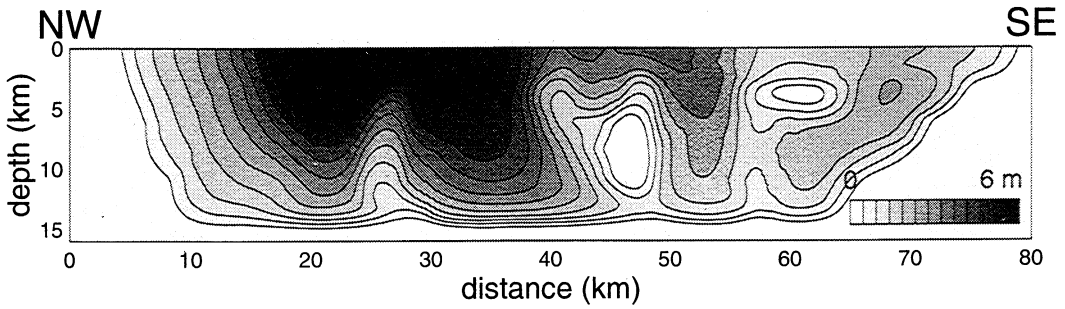

Figure 5. Slip distribution on the fault for our preferred dynamic model of the Landers 1992 earthquake. Contour interval is 0.5 m.

of the spatial heterogeneities of the initial stress distribution. The rupture front is arrested when it enters into an unstressed patch or a previously broken patch on the fault. Here the stress increases as the rupture front penetrates into the patch, and stress drop is actually negative, as predicted by *Husseini et al.* [1975].

Figure 5 shows the final slip distribution on the fault. Our dynamic rupture model reproduces the general slip pattern used to compute the initial stress distribution, even if the resulting slip distribution is smoother than the prestress distribution. We think that this slip distribution is realistic because the maximum slip is confined to the shallow portion at the end of the fault, in the Camp Rock-Emerson Valley segment, in agreement with observed surface offset [*Sieh et al.*, 1993]. The distribution of cumulative slip projected to the main rupture trace as determined by *Sieh et al.* [1993] shows a maximum surface slip of ~6 m near the end of the fault. Slip near the hypocenter was smaller and occurred at greater depths. Regions with small slip are juxtaposed against regions of much higher slip because of dynamic instabilities in the rupture process and stress heterogeneities. The regions of the fault where slip is large are also the regions where there is a high-stress drop and conversely, as shown previously by *Bouchon* [1997] for other earthquakes of the San Andreas system.

Figure 6 shows the slip-rate integrated across the fault depth as a function of time, representing the average rupture front propagation. When the rupture propagates from a region of low stress to a region of high-stress concentration, near 13 s, for instance, the rupture velocity increases. Thus the peak slip near the surface is associated with a supershear speed of rupture, an effect that is enhanced by the free surface. The first report of locally supershear rupture velocities is due to *Archuleta* [1984], but such supershear transition is rarely observed in earthquakes because of the low resolution of data. Another explanation for this small number of observations of supershear rupture speeds is that the stress distribution in the fault zone is very heterogeneous, and only isolated patches of the fault are highly stressed. The subshear rupture velocities generally occur within and near the low-stress areas on the fault while supershear ones dominate within very highly stressed patches of the fault where the rupture resistance is relatively low and κ is very large compared to its critical value. Supershear velocities are particularly important near the surface. Indeed, the rupture velocity shows a strong variation during this earthquake for the dynamic simulation. If the rupture front encounters a

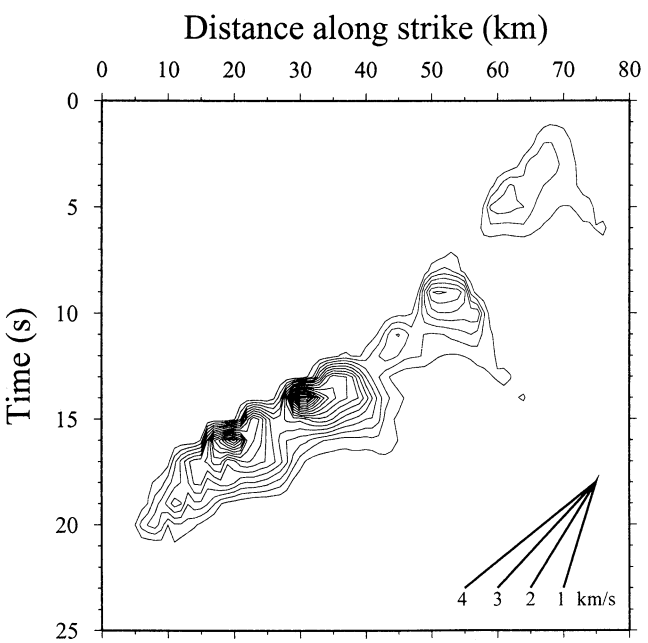

Figure 6. Contours of depth-averaged slip rate as a function of position along strike and time for our final dynamic model of the 1992 Landers earthquake. The slopes of the slanted lines depict a range of rupture velocities.

Table 2. Stations From California Division of Mines and Geology (CMDG) California Strong Motion Program Used in our Dynamic Models

Station Name	Station Location	Epicentral Distance, km	Closest Distance to Fault, km
BKR	Baker	123.9	85.0
BRN	Boron	142.5	99.3
BRS	Barstow	94.7	44.4
FTI	Fort Irwin	120.9	66.8
H05	Hemet Fire Station	72.6	70.1
INI	Indio	59.7	54.3
PSA	Palm Springs	41.8	37.1
PWS	Twentynine Palms	44.2	40.5
YER	Yermo	85.8	31.0

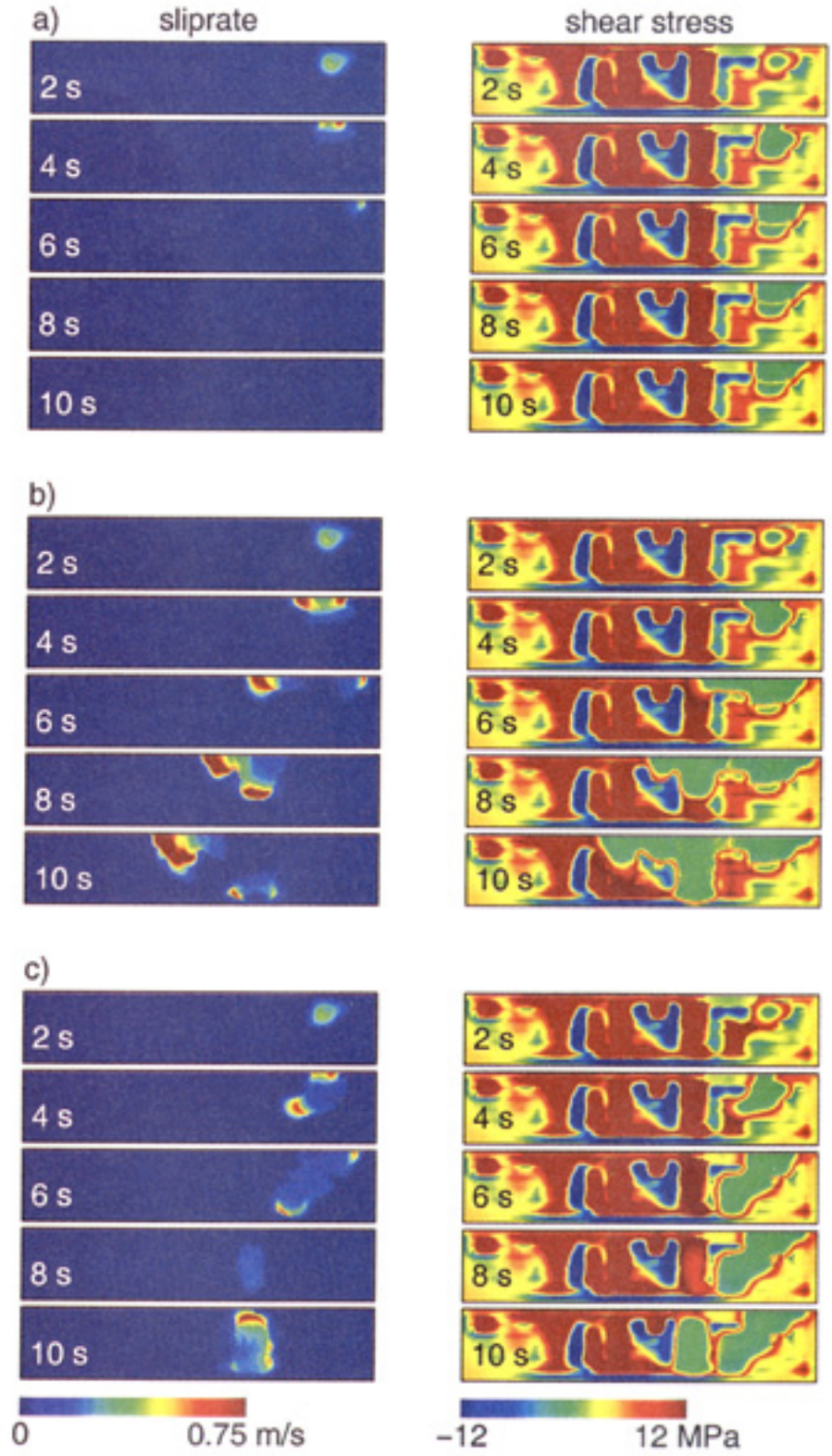

Plate 1. Influence of the prestress: rupture history for three different initial conditions of shear stress on the Landers fault. (a) Rupture starts but stops after 6 seconds, and (b and c) rupture propagates but follows different paths.

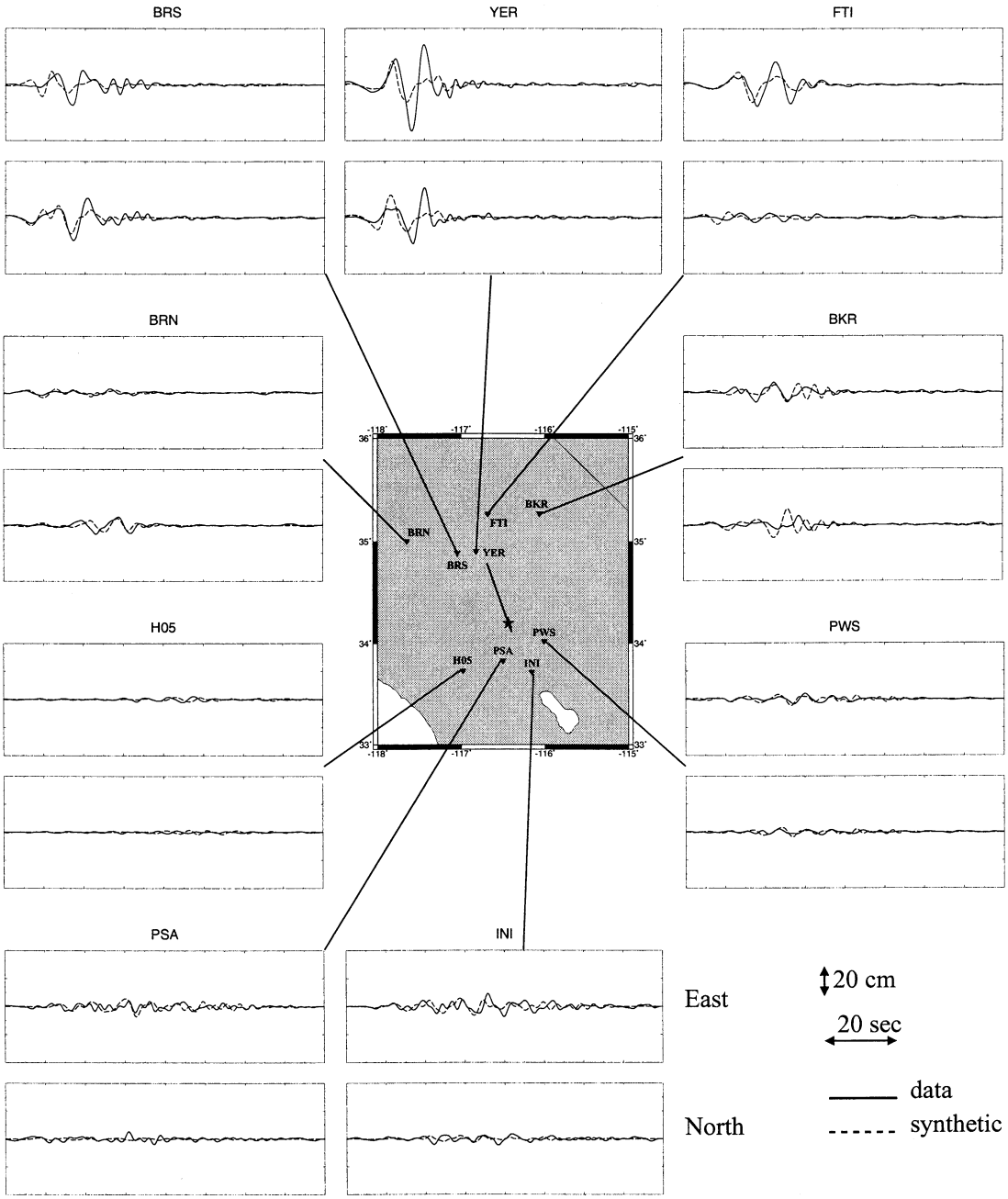

Figure 7. Comparison between observed ground displacements and those obtained for the starting model of the 1992 Landers earthquake [*Olsen et al.*, 1997]. For each station the upper trace is the east-west component of displacement, and the bottom trace is the north-south component. The time window is 80 s, and the amplitude scale is the same for all stations.

high-stress patch, it will change its rupture velocity instantaneously. However, on average, rupture propagates with a velocity of ~2.7 km/s, in agreement with the constant velocity implied in the kinematic model. Thus this model reproduces the total rupture time and the final slip distribution obtained by *Wald and Heaton* [1994] by kinematic inversion. Besides, the seismic moment found for our dynamic model is $M_0 = 0.7 \times 10^{20}$ N m, which corresponds to $M_w = 7.17$, in agreement with the value for the kinematic model ($M_w = 7.2$) [*Wald and Heaton*, 1994] and with geological estimation ($M_w = 7.3$) [*Sieh et al.*, 1993].

4.2. Success of the Dynamic Inversion

The heterogeneous rupture propagation in our model of the Landers earthquake generates strong seismic radiation. In the following we will analyze the waves radiated by our dynamic model in the near field because the far field does not have enough resolution to reveal details of the rupture propagation and, in particular, the healing of slip. These data are also less sensitive to velocity and attenuation heterogeneity in the source-receiver path than are the teleseismic recordings at comparable frequencies. The strong motion

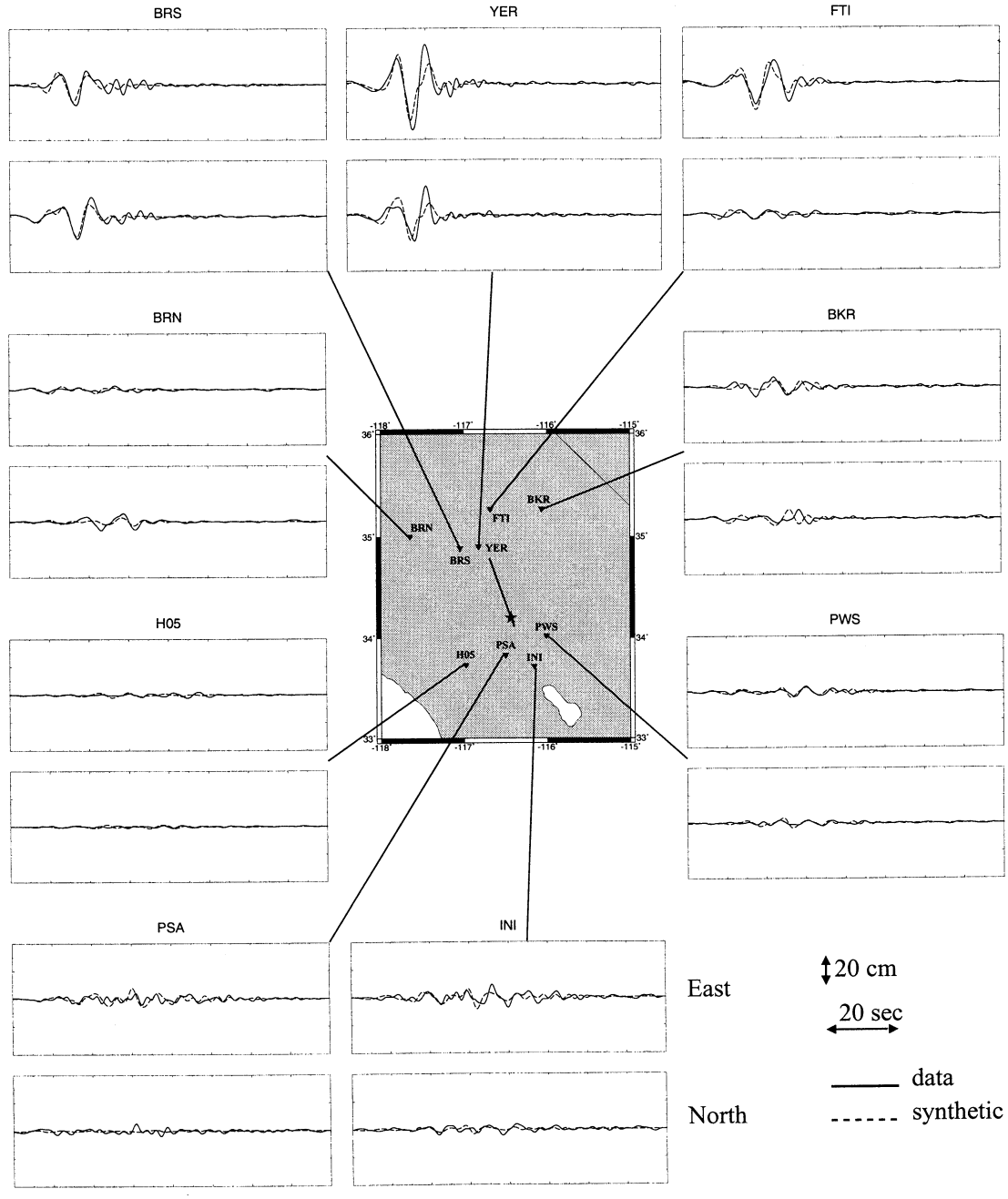

Figure 8. Same as Figure 7, but for our preferred dynamic model.

stations (Table 2), located at distances from 40 to 150 km, provide a unique data set for determining the source characteristics. Owing to the large distance from the fault to some of the strong motion stations the computation of radiation using the FD method is relatively expensive. For this reason we generated synthetic ground motion from our dynamic simulation with the less computationally demanding discrete wave number method of *Bouchon* [1981], in which the reflection-transmission matrices of *Kennett and Kerry* [1979] are used. The fault is divided into subfaults with individual slip history, determined from the dynamic simulation. The Green's function for every source-receiver pair are convolved by the appropriate source time functions.

The observed seismic waveforms are an integral property of the slip distribution, and measurements of the slip parameters are themselves averages, temporal in the case of dynamic measurements. We focused our attention on S waves because the horizontal components have a lower-frequency content than the vertical components. Furthermore, they show less indications of phase conversions and propagation complexity, which is necessary for the use of a one-dimensional crustal structure. The displacement ground motions are relatively long period, dominated by 3-10 s waves. Our numerical method enables us to model frequencies only up to 0.5 Hz because of limitations in resolution of the dynamic model. Thus both synthetics and data were band-pass

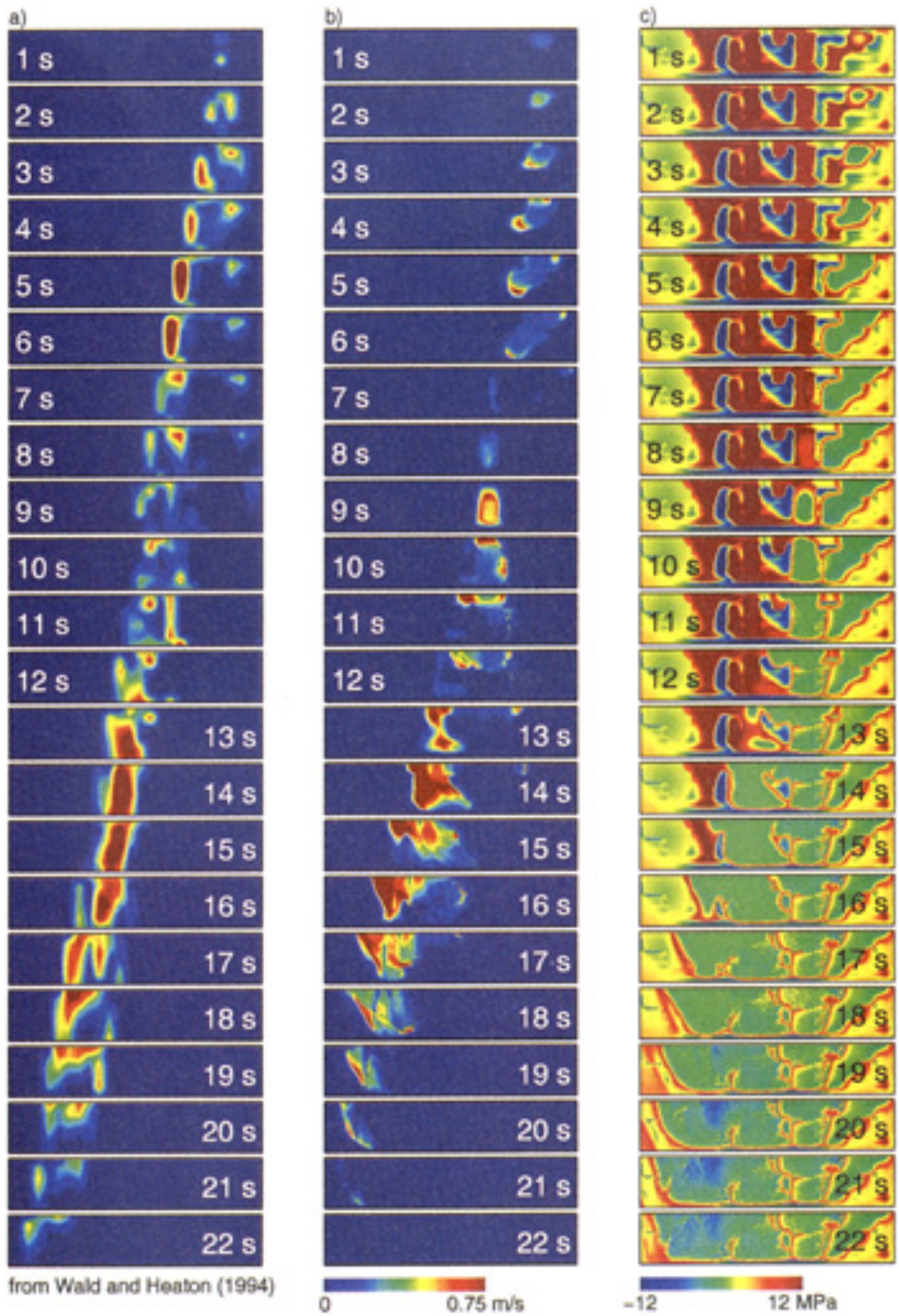

Plate 2. Snapshots of (a) the kinematic model recomputed from *Wald and Heaton* [1994] compared to (b) our dynamic rupture simulation of the 1992 Landers earthquake on the fault plane. The snapshots depict the horizontal slip rate in 1 s time slices. (c) Shear stress on the Landers fault as a function of time for our preferred dynamic rupture model described in Plate 2b. The propagation is associated with a stress decrease (green), and the rupture only propagates in regions of high stress (red).

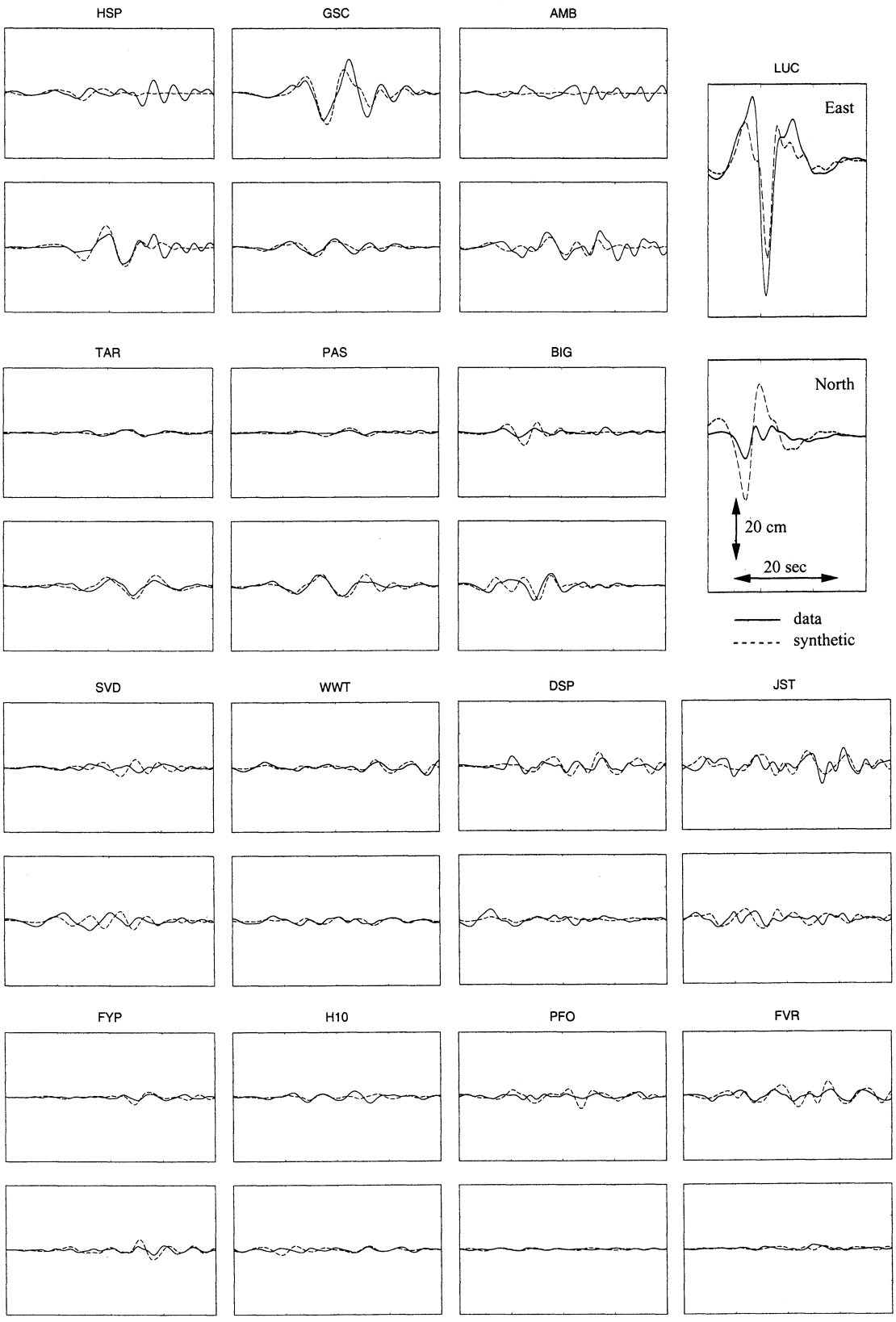

Figure 9. Comparison between observed ground displacements and those obtained for our dynamic model of the 1992 Landers earthquake. For each station the upper trace is the east-west component of displacement, and the bottom trace is the north-south component. The time window is 40 s, except for station LUC, which is 30 s, and the amplitude scale is the same for all stations.

filtered between 0.07 and 0.5 Hz with a zero-phase, third-order Butterworth filter and then doubly integrated to obtain displacements.

Figure 7 shows a comparison between observed ground displacements and the synthetics obtained for the starting model of *Olsen et al.* [1997], and Figure 8 shows a comparison for our final dynamic rupture history. Clearly, we obtain an improved fit with our final model (Figure 8). The scale is the same for all stations, so that the rupture directivity of the source can be clearly seen in the records from PWS (Δ = 44.2 km) located to the south and YER (Δ = 85.8 km) located to the north of the epicenter. The peak displacement shows a different pattern for these two stations, reflecting the rupture directivity from south to north: the maximum displacement at PWS is only 16% of that at YER despite the shorter epicentral distance to PWS than to YER. Rupture is seen to be largely unilateral northward, causing a high-amplitude shear pulse in this direction. The best fit is obtained for stations BRS, YER, and FTI in the forward rupture direction. Stations H05, PSA, INI, and PWS are located in the direction opposite of rupture propagation, causing displacement amplitude to be smaller than at the other stations. For example, at H05, there is no clear pulse to fit; however, the computation succeeds in predicting the peak amplitudes. Discrepancies in the backward direction are due to a higher relative influence of crustal structure. In this case the effect of propagation path between source and receiver becomes more important than the effect of the source. This is particularly the case for stations PSA and INI, which show strong complexity in phase arrivals, and the modeling becomes more difficult. Likewise, the influence of the simple one-dimensional model is increased by the large distance from the fault to some stations. Nevertheless, overall waveforms are well reproduced by the synthetics, confirming that our dynamic inversion converged to a realistic rupture model.

Table 3. Stations Used in the Validation of our Dynamic Models, Recorded by California Institute of Technology (CIT), California Strong Motion Program (CDMG), Southern California Edison (SCE), and U.S. Geological Survey (USGS)

Station Name	Station Location	Epicentral Distance, km	Closest Distance to Fault, km
AMB	Amboy	75.2	73.2
BIG	Big Bear	46.3	42.6
DSP	Desert Hot Springs	27.4	23.1
FVR	Fun Valley	31.0	25.8
FYP	Featherly Park	123.1	122.7
GCS	Goldstone Lake	126.4	72.0
H10	Silent Valley	54.7	52.4
HSP	Hesperia	83.4	69.1
JST	Joshua Tree	13.7	10.0
LUC	Lucerne Valley	42.0	2.0
MVF	Morongo Valley	21.0	18.9
PAS	Pasadena	159.7	151.5
PFO	Pinyon Flat Obs.	64.6	60.4
SVD	Seven Oaks Dam	61.1	60.7
TAR	Tarzana	193.2	182.4

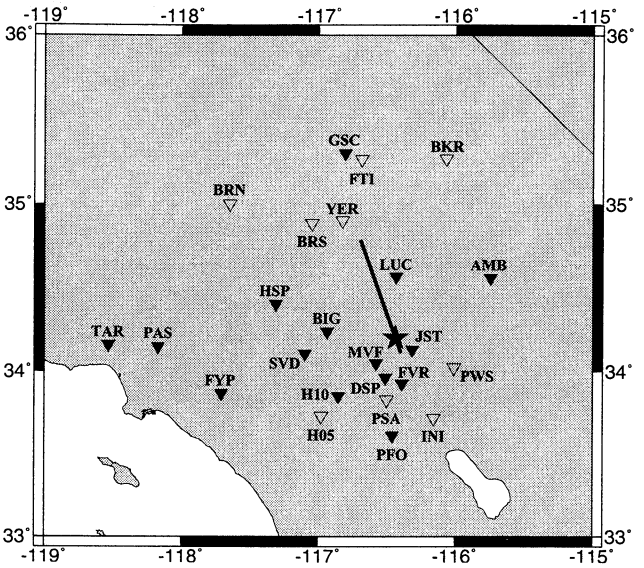

Figure 10. Map of southern California. Stations used in the validation of the dynamic model found are depicted by solid triangles, and open triangles represent the stations used in the trial-and-error inversion. The star depicts the epicenter of the 1992 Landers earthquake.

Slip in the epicentral region is mostly controlled by the local stress drop, while slip near the end of the fault is controlled by a wider window of radiation. Thus information from earlier rupture propagation arrives at the same time as local information, its importance decreasing inversely with distance from the source. Consequently, the information contained in the data is mainly radiation from the last part of the Landers earthquake (corresponding to 13-17 s in Plate 2).

5. Further Validation of the Model

In the previous sections we inverted the initial stress field on the Landers fault by a trial-and-error method using nine near-field strong motion stations. The solution we found is one of a series of possible dynamic rupture solutions. In order to test the robustness of the inverted solution we generated synthetics at a set of additional 15 stations. While these stations were not used to invert the initial stress field, we simply applied the dynamic rupture model obtained in the our previous inversion to propagate the radiation to the additional stations.

Figure 9 shows a comparison between observed ground displacements and synthetics obtained for our final dynamic model. The stations from different institutions are listed in Table 3. The station coverage is quite complete in azimuth and distance (stations range from 13.7 to 193.2 km, see Figure 10). Synthetics and data were processed similarly to the procedure described for inversion. The data are well reproduced by the synthetics for almost all the stations. We think that the discrepancies are mainly due to the effects of propa-

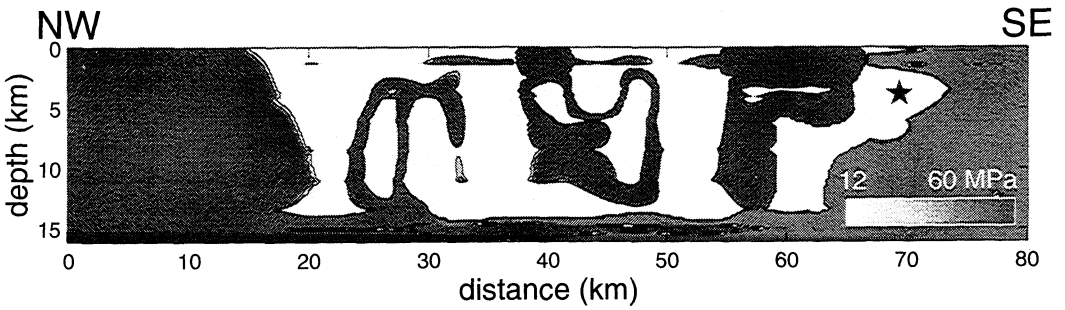

Figure 11. Yield stress field on the Landers fault obtained for the heterogeneous yield stress model calculated from the asperity model.

gation in a laterally heterogeneous medium, which were not modeled by our 1-D structure. Station LUC (Lucerne Valley) poses a different problem because it was located very close to the fault trace at intersection between two segments. Since, as we explained earlier, we had to simplify the fault so that it is a single plane, the station is no longer located near the fault trace in our model.

We conclude from Figure 9 that our dynamic model is compatible with the available data. This solution is preferable for a model in which only initial stress is heterogeneous, all other parameters being uniform on the fault. We will refer to this model as the asperity model. There is some evidence by *Ide and Takeo* [1997], that the slip-weakening distance in the shallower parts of the crust tends to be larger than at depth. Such variation could be due to the increase of elastic rigidity with depth. An interesting alternative to the asperity model is to study a model where initial stress is uniform while rupture resistance varies locally. Following seismological practice, we will call this the barrier model.

Madariaga and Olsen [2000] showed that we can understand propagation of rupture in terms of a nondimensional parameter κ (see (5)). For low values of κ, rupture does not propagate because the Griffith's criterion is not satisfied. A bifurcation occurs when κ crosses a critical value κ_c, so that rupture grows whenever κ is larger than critical. Using (5) for κ, we can generate a complementary model of variable yield stress and constant initial stress over the fault. The characteristic length scale W and the slip-weakening distance D_c which appeared in the expression for the parameter κ are assumed to be the same for both the asperity and the barrier models. Wherever rupture could propagate in the asperity model, rupture must also propagate in the barrier model because the value of κ is identical in both models. As well as for the previous model, we used a trial-and-error method in order to improve the stress resistance model. In the inversion we assumed that the initial stress field was uniform over the fault and equal to $T_e = 12$ MPa. The slip-weakening distance was the same as for the asperity model, $D_0 = 0.8$ cm.

Figure 11 shows the yield stress calculated by the method explained earlier and modified by trial-and-error inversion. The yield stress T_u reproduces the general pattern of the initial stress used to compute it, but its variations are more abrupt, and values in general are higher than for the asperity model. The slip distribution produced by this model is shown in Figure 12. There are no major differences compared to the asperity model (Figure 5) even though initial conditions are completely different. The maximum slip is confined to the shallowest part of the fault in Camp Rock-Emerson Valley segment, in agreement with surface offset and with the previous model. In contrast, slip is, again, deeper and lower in the region near the hypocenter. Of course, this slip distribution is smoother than for the asperity model, and it could be improved by additional trial-and-error cycles. In this case the seismic moment found is $M_0 = 0.56$ x 10^{20} N m, which corresponds to a magnitude $M_w = 7.1$. Finally, Figure 13 shows the comparison between ground displacement for data and synthetics calculated from the rupture history obtained for this second model. The overall waveforms are well reproduced by the synthetics, and once again, the best fits are obtained for stations in the forward rupture direction (YER, BRS, and FTI).

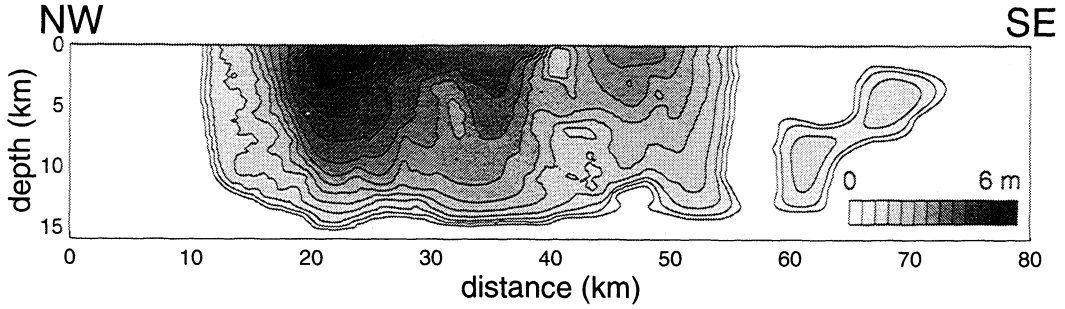

Figure 12. Slip distribution on the Landers fault for the barrier model of the 1992 Landers earthquake. Contour interval is 0.5 m.

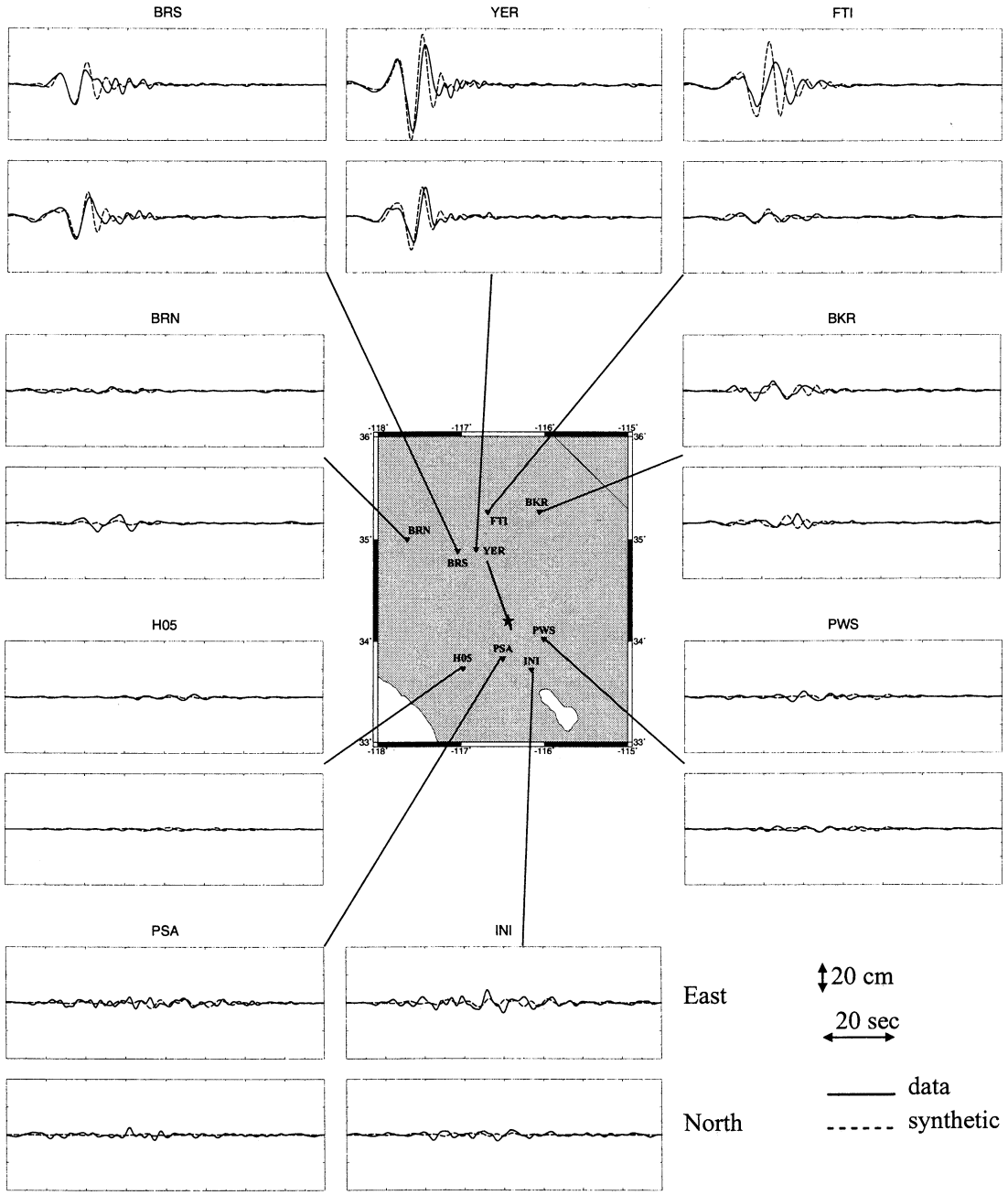

Figure 13. Same as Figure 8, but for the barrier model.

The fit is even better than for the asperity model; for example, the second pulse is better reproduced than that in Figure 6. In summary, we have found another valid dynamic model of the Landers earthquake which reproduces the slip distribution and fits data.

6. Discussion

It should be noticed how important a well-constrained kinematic starting model is in order to obtain a good dynamic model, with a small number of trial-and-error tests. Despite the constraints on resolution we obtain an improved fit between dynamic radiation and strong motion data. Thus we have generated a complex dislocation distribution on the fault surface with a simple slip-weakening friction law and a realistic, heterogeneous initial stress distribution inverted by a trial-and-error method. The rupture propagation from the initial asperity patch, the rupture speed, and the healing are critically determined by the friction parameters [*Madariaga and Olsen*, 2000] but also, as shown in this study, by the distribution of prestress. Consequently, a critical balance between initial stress and frictional parameters has to be met in order to generate a rupture history and a final slip distribution that follow those determined by kinematic inversion.

Since our method is currently limited to planar faults, the approximation of a single fault plane is an important dif-

ference with the kinematic inversion by *Wald and Heaton* [1994], where the fault was subdivided into three segments. Nevertheless, since the resolution of ground motion is ~5 km (corresponding to ~0.5 Hz), the influence of the segmentation is probably not very important. However, a more realistic geometry could be a challenging implementation, especially if the maximum frequency of the numerical method is increased. However, this requires increased spatial resolution and therefore an improved crustal model. Dynamic modeling of high frequencies could provide more information about the dynamics of rupture, resolving details of the dynamic stress drop, and rupture velocities. *Wald and Heaton* [1994] found a slower rupture velocity for the shallower part of the fault compared to our dynamic simulation where the velocity tends to be supershear near the surface. The free surface is found to have a strong effect on dynamic rupture propagation. Moreover, the nature of rupture arrest, especially in the deeper part of the Landers fault, is different for the dynamic and kinematic results. The kinematic solution shows an abrupt stop of slip, which is unphysical, whereas the dynamic rupture front is arrested because it penetrates into the unstressed area at the bottom of the fault. This implies that the stress drop distribution should taper away to the north and to the bottom of the fault in a physically reasonable manner. This is a dynamic effect, which cannot be determined with kinematic models.

We have showed that the solution to the inverse problem of dynamic rupture propagation is nonunique. Indeed, we found two very different dynamic models that fit the data almost equally well. One was an asperity model in which everything except initial stress was uniform; the other was a barrier model where everything was uniform except rupture resistance. We succeeded in inverting the Landers displacement data with both models, confirming our earlier hypothesis that seismic data cannot distinguish between barriers and asperities [see *Madariaga*, 1979]. It is important to point out that we see no clear indications in the data as to which model is better. The real solution must then be somewhere between these two extremes. Consequently, only the ratio of available strain energy to fracture energy, which is the physical meaning of parameter κ, can be used to describe the rupture propagation.

An important goal in dynamic studies is to determine the rupture process as an inverse problem given a certain number of seismic observations. Dynamic source parameters are often difficult to estimate because of their strong nonlinearity [*Guatteri and Spudich*, 2000]. Our results suggest that modeling of the prestress and frictional parameters can lead to increased knowledge of the rupture process. The strong sensitivity of the radiation to the stress distribution shows promise for future inverse modeling in order to better constrain dynamic rupture parameters.

7. Conclusions

We have modeled the dynamic rupture of Landers earthquake with a trial-and-error method with two complementary models, a barrier and an asperity model, assuming either variable initial stress or variable yield stress. Both models successfully fit the rupture history and the duration of the Landers earthquake determined from kinematic inversion without introducing any major changes in the distribution of fault slip. The overall kinematics are similar to those determined by *Wald and Heaton* [1994], *Cohee and Beroza* [1994], and *Cotton and Campillo* [1995]. We also obtained similar moment and slip distribution as in their models, and we fit the observed ground displacements very satisfactorily. Thus we constructed two well-posed mechanical models of the Landers earthquake that satisfy available seismological data. These models are end-members of a large family of dynamically correct models. We suggest that the proper way to characterize these models is the local nondimensional parameter κ introduced by *Madariaga and Olsen* [2000]. The next step is to use a segmented model that will also satisfy geodetic observations, which are more sensitive to the geometry of the fault, especially for GPS stations located near the change of strike of the fault.

Acknowledgments. We thank Bruno Hernandez for his help on using the program AXITRA and numerous discussions. The computations in this study were carried out on the facilities of the Département de Modélisation Physique et Numérique de l'Institut de Physique du Globe de Paris. This research work was supported by grants from the Programme National des Risques Naturels of the Institut National de Sciences de l'Univers du CNRS (S.P. and R.M.) and by the Southern California Earthquake Center (SCEC). SCEC is funded by NSF cooperative agreement EAR-8920136 and USGS cooperative agreements 14-08-0001-A0899 and 1434-HQ-97AG01718 (K.B.O). This is ICS contribution 362-105EQ and SCEC contribution 554.

References

Andrews, J., Rupture velocity of plane strain shear cracks, *J. Geophys. Res.*, *81*, 5679–5687, 1976.

Aochi, H., Theorical studies on dynamic rupture propagation along a 3D non-planar fault system, Ph.D. thesis, Univ. of Tokyo, Tokyo, 1999.

Aochi, H., and E. Fukuyama, Selectivity of spontaneous rupture propagation on a branched fault, *Geophys. Res. Lett.*, *27*, 3635–3658, 2000.

Aochi, H., E. Fukuyama, and R. Madariaga, Effect of normal stress on a dynamic rupture along a non-planar fault, *Eos Trans. AGU*, *84*, Fall Meet. Suppl., F1227, 2000.

Archuleta, R., A faulting model for the 1979 Imperial Valley earthquake, *J. Geophys. Res.*, *89*, 4559–4585, 1984.

Beroza, G. C., and T. Mikumo, Short slip duration in dynamic rupture in the presence of heterogeneous fault properties, *J. Geophys. Res.*, *101*, 22,449–22,460, 1996.

Bouchon, M., A simple method to calculate Green's function for layered media, *Bull. Seismol. Soc. Am.*, *71*, 959–971, 1981.

Bouchon, M., The state of stress on some faults of the San Andreas system as inferred from near-field strong motion data, *J. Geophys. Res.*, *102*, 11,731–11,744, 1997.

Bouchon, M., M. Campillo, and F. Cotton, Stress field associated with the rupture of the 1992 Landers, California, earthquake and its implications concerning the fault strength at the onset of the earthquake, *J. Geophys. Res.*, *103*, 21,091–21,097, 1998.

Cohee, B., and G. Beroza, Slip distribution of the 1992 Landers earthquake and its implications for earthquake source mechanics, *Bull. Seismol. Soc. Am.*, *84*, 692–712, 1994.

Cotton, F., and M. Campillo, Frequency domain inversion of strong motions: Application to the 1992 Landers earthquake, *J. Geophys. Res.*, *100*, 3961–3975, 1995.

Day, S., Three-dimensional simulation of spontaneous rupture: the effect of nonuniform prestress, *Bull. Seismol. Soc. Am.*, *72*, 1881–1902, 1982.

Day, S. M., G. Yu, and D. J. Wald, Dynamic stress changes during earthquake rupture, *Bull. Seismol. Soc. Am.*, *88*, 512–522, 1998.

Freund, L., *Dynamic Fracture Mechanics*, Cambridge Univ. Press, New York, 1989.

Fukuyama, E., and T. Mikumo, Dynamic rupture analysis: Inversion of the source process of the 1990 Izu-Oshima, Japan earthquake (M=6.5), *J. Geophys. Res.*, *98*, 6529–6542, 1993.

Guatteri, M., and P. Spudich, What can strong-motion data tell us about slip-weakening fault-friction laws?, *Bull. Seismol. Soc. Am.*, *90*, 98–116, 2000.

Harris, R., and S. Day., Dynamics 3D simulations of earthquakes on an echelon faults, *Geophys. Res. Lett.*, *26*, 2089–2092, 1999.

Hernandez, B., F. Cotton, and M. Campillo, Contribution of radar interferometry to a two-step inversion of the kinematic process of 1992 Landers earthquake, *J. Geophys. Res.*, *104*, 13,083–13,099, 1999.

Husseini, M. I., D. B. Jovanovich, M. J. Randall, and L. B. Freund, The fracture energy of earthquakes, *Geophys. J. R. Astron. Soc.*, *43*, 367–385, 1975.

Ida, Y., Cohesive force across the tip of a longitudinal-shear crack and Griffith's specific surface energy, *J. Geophys. Res.*, *77*, 3796–3805, 1972.

Ide, S., and M. Takeo, Determination of constitutive relations of fault slip based on seismic wave analysis, *J. Geophys. Res.*, *102*, 27,379–27,392, 1997.

Kennett, B. L., and N. J. Kerry, Seismic waves in a stratified half space, *Geophys. J. R. Astron. Soc.*, *57*, 557–583, 1979.

Madariaga, R., Dynamics of an expanding circular fault, *Bull. Seismol. Soc. Am.*, *66*, 639–666, 1976.

Madariaga, R., On the relation between seismic moment and stress drop in the presence of stress and strengh heterogeneity, *J. Geophys. Res.*, *84*, 2242–2250, 1979.

Madariaga, R., and K. Olsen, Criticality of rupture dynamics in 3-D, *Pure Appl. Geophys.*, *157*, 1981–2001, 2000.

Madariaga, R., K. Olsen, and R. Archuleta, Modeling dynamic rupture in a 3D earthquake fault model, *Bull. Seismol. Soc. Am.*, *88*, 1182–1197, 1998.

Miyatake, T., Reconstruction of dynamic rupture process of an earthquake with constraints of kinematic parameters, *Geophys. Res. Lett.*, *19*, 349–352, 1992.

Nielsen, S. B., and K. B. Olsen, Constraints on stress and friction from dynamic rupture models of the 1994 Northridge, California earthquake, *Pure Appl. Geophys.*, *157*, 2029–2046, 2000.

Olsen, K., Simulation of three-dimensional wave propagation in Salt Lake Basin, Ph.D. thesis, Univ. of Utah, Salt Lake City, 1994.

Olsen, K., R. Madariaga, and R. Archuleta, Three dimensional dynamic simulation of the 1992 Landers earthquake, *Science*, *278*, 834–838, 1997.

Peyrat, S., K. Olsen, and R. Madariaga, Dynamic modeling of the Landers earthquake with spatially variable friction, *Eos Trans. AGU*, *84*, Fall Meet. Suppl., F1239, 2000.

Quin, H., Dynamic stress drop and rupture dynamics of the October 15, 1979 Imperial Valley, California, earthquake, *Tectonophysics*, *175*, 93–117, 1990.

Sieh, K., et al., Near field investigation of the Landers earthquake sequence, April to July, 1992, *Science*, *260*, 171–176, 1993.

Unruh, J. R., W. R. Lettis, and J. M. Sowers, Kinematic Interpretation of the 1992 Landers Earthquake, *Bull. Seismol. Soc. Am.*, *84*, 537–546, 1994.

Virieux, J., and R. Madariaga, Dynamic faulting studied by a finite difference method, *Bull. Seismol. Soc. Am.*, *72*, 345–369, 1982.

Wald, D., and T. Heaton, Spatial and temporal distribution of slip for the 1992 Landers, California, earthquake, *Bull. Seismol. Soc. Am.*, *84*, 668–691, 1994.

R. Madariaga and S. Peyrat, Laboratoire de Géologie, École Normale Supérieure, 24 rue Lhomond, 75231 Paris Cedex 05, France. (e-mail: madariag@geologie.ens.fr; peyrat@geologie.ens.fr)

K. Olsen, Institute for Crustal Studies, UC Santa Barbara, Santa Barbara, CA 93106, USA. (e-mail: kbolsen@crustal.ucsb.edu)

(Received August 1, 2000; revised June 8, 2001;
accepted June 9, 2001.)